IJMCM
Winter 2020, Vol 9, No 1
DOI: 10.22088/IJMCM.BUMS.9.1.90

Original Article

Computational Approach for Rational Design of Fusion Uricase with PAS Sequences

Abbas Najjari[1], Hamzeh Rahimi[2], Seyed Ali Nojoumi[3], Eskandar Omidinia[1*]

1. Enzyme Technology Laboratory, Department of Biochemistry,Genetic and Metabolism Research Group, Pasteur Institute of Iran,Tehran, Iran.

2. Molecular Medicine Department, Pasteur Institute of Iran, Tehran, Iran.

3. Microbiology Research Center, Pasteur Institute of Iran, Tehran, Iran.

Tumor lysis syndrome is a life-threatening condition for humans due to the lack of urate oxidase. In this study, several variants of PASylated uricase from the *Aspergillus flavus* species were analyzed computationally to find the appropriate fusions to solve short half-life and stability concern. The *Ab initio* method was performed using Rosetta software to structurally characterize the PAS sequences. The 3D structures of fusions were predicted for fused C- or N-terminally PAS sequences in different length to the uricase. The refinement and energy minimization steps revealed that physicochemical and conformational properties of fusions improved while the structures possessed prolonged PAS sequences. Molecular docking results showed that the highest binding affinity to uric acid belonged to uricase-PAS1-100 by the formation of six hydrogen and four non-hydrogen bonds. Altogether, the results indicated that the PASylation process would be promising upon the production of urate oxidase with improved solubility and stability.

Key words: Tumor lysis syndrome, *Aspergillus flavus*, uricase, molecular dynamic, PASylation, plasma half-life

Tumor lysis syndrome (TLS) indicates the metabolic events caused by massive tumor cell lysis leading to the release of intracellular contents into the bloodstream (1-3). TLS may occur spontaneously or in response to therapy that results in hyperuricemia, hyperkalemia, hyperphosphatemia, and hypocalcemia (4, 5). Often, hyperuricemia or a uric acid level more than 8 mg/dL can lead to acute renal failure (6, 7). Besides, catabolism of purine nucleic acids in lysed tumor cells accompanied by conversion to hypoxanthine and xanthine contribute to boosting the uric acid catalyzed by xanthine oxidase (8).

Traditionally, there are standard strategies for the prevention and treatment of the TLS-associated metabolic abnormality including hydration, alkalinization of the urine with sodium bicarbonate, and allopurinol (9). As the xanthine oxidase inhibitor allopurinol only prevents the formation of uric acid, it does not degrade the uric acid prior to treatment (10). Conversion of uric acid to allantoin, a more water-soluble form, by urate oxidase (UO)

*Corresponding author: Enzyme Technology Laboratory, Department of Biochemistry,Genetic and Metabolism Research Group, Pasteur Institute of Iran,Tehran, Iran. Email: eomid8@gmail.com

This work is published as an open access article distributed under the terms of the Creative Commons Attribution 4.0 License (http://creativecommons.org/licenses/by-nc/4). Non-commercial uses of the work are permitted, provided the original work is properly cited.

[Downloaded from ijmcmed.org on 2026-11-12]

[DOI: 10.22088/IJMCM.BUMS.9.1.90]

is an alternative approach to inhibit uric acid formation (11). UO is a key enzyme that exists commonly in many mammalian species but is inactive in humans owing to two nonsense mutations in the coding region during hominoid evolution (12, 13).

Recently, a recombinant UO (rasburicase) has been derived from the coding gene of the *Aspergillus flavus* species. The homotetrameric enzy me contains 301 residues that are expressed in a genetically modified *Saccharomyces cerevisiae* strain (14). Rasburicase was approved by the European medicines agency under the name of Fasturtec® in 2001 and by the US Food and Drug Administration (FDA) under the name of Elitek® in 2002 for treatment of hyperuricemia during chemotherapy (15, 16).

Although, rasburicase was well tolerated and showed significant reduction in serum uric acid concentration versus allopurinol (87% vs 66%), there were some drawbacks that affected its efficacy (17). In general, the immunogenicity, short half-life of 18-21 h and the cost of rasburicase led to propose poly ethylene glycol (PEG)ylation technique (18). In 2010, pegloticase (Krystexxa), a PEGylated form of UO was approved by FDA to have a prolonged half-life of 10-20 days, and reduced immunogenicity. Despite the fact that the development of anti-PEG antibodies has been reported (19), expensive downstream processing steps of PEGylation and non-degradability of PEG have limited this strategy (20).

Nowadays, the biological alternative to PEGylation are those sequences comprising the three small amino acids Pro, Ala, and Ser (PAS) (20). Such sequences show high stability and solubility in physiological condition but no immunogenicity. Furthermore, the mixtures of the selected amino acids, particularly Pro, provide random coil structures formation, which result in increasing the hydrodynamic volume. Finally, the uncharged PAS sequences show no interference with the pharmacological activity of the drugs (21). PASylation, as a simple and easy technique has successfully been applied to increase the half-life of conjugated therapeutic drugs, including hormones, cytokines, antibody fragments, and enzymes (22). However, the adjustment of the polypeptide sequence and length should be considered to avoid the generation of secondary structures.

In the search for improvement of the biostability of uricase from *Aspergillus flavus*, we have computationally generated several uricase-PAS fusions through combinations of different PAS polypeptides whose physicochemical properties and activity of structures were evaluated *in silico*. Our findings would provide new insights into the production of uricase with improved solubility, stability, and biological activity.

Materials and methods

Multiple sequence alignment

The corresponding amino acid sequences of uricase in several species of *Aspergillus* were retrieved from Refseqprotein of NCBI (https://www.ncbi.nlm.nih.gov/). Multiple sequence alignment was carried out using Clustal Omega (23), and visualized by Jalview (24). The phylogenetic tree was constructed based on the neighbor joining method with boot strapping using MEGA7.0 (25). Some sets of the PAS sequences having different building blocks were obtained from the patents and studies (Table 1). In order to identify the repetitive blocks of PAS sequences, multiple sequence alignment was performed using Clustal Omega. These blocks were utilized to design several PAS sequences with different length.

Calculation of physicochemical properties

The physicochemical properties of designed PAS sequences, including molecular weight (MW), pI, charge at pH 7, residues composition, instability index, and grand average of hydropathicity (GRAVY) were calculated using Expasy's ProtParam and Protein Calculator v3.4 (PepCalc)

[Downloaded from ijmcmed.org on 2026-11-12]

[DOI: 10.22088/IJMCM.BUMS.9.1.90]

Table 1. The repetitive blocks of PAS sequences.

Block ID	Sequence
PAS#1	ASPAAPAPASPAAPAPSAPA
PAS#2	AAPASPAPAAPSAPAPAAPS
Modified PAS#3	SAPSSPSPSAPSSPSPASPS
PAS#3 non-modified	APSSPSPSAPSSPSPASPSS
PAS#4	SSPSAPSPSSPASPSPSSPA
PAS#5	AASPAAPSAPPAAASPAAPSAPPA
PAS#6	ASAAAPAAASAAASAPSAAA

web tools (26, 27).

***Ab initio* molecular modeling of PAS sequences**

The structure of PAS sequences was predicted by *ab initio* approach using Rosetta 3.4 package (28). Fragment libraries of three- and nine-residues were created by Robetta fragment server (29). Predicted secondary structure of fragments using Jpred (30) and their sequences in FASTA format were as input files to generate 100,000 initial structures for each sequence using Abinitio Relax command (31). The resulting output contained the PDB models and Rosetta score information in a compact format. The models were sorted by total score, then the best-predicted structures based on their energy were refined using idealize command.

Modeling, refinement and quantitative evaluation of fusion proteins

The amino acid sequence of uricase from *Aspergillus flavus* was submitted to HHpred to achieve a suitable template structure (32). The crystal structure of uricase protein with 1.4Å resolution was retrieved from the existing crystal structure (4D12) in the RCSB protein data bank (PDB). Protein sequence search of this template with uricase resulted in 100% and 1.447 identity and similarity, respectively. To perform modeling predictions of the full length of uricase-PAS sequences, the best *Ab initio* generated PAS model of each sequence was merged with the template crystal structure. Modeller software version 9.11 was employed to make 10,000 models using each of these new templates. Based on the ranked discrete optimized potential energy (DOPE) score of generated models, ten top predicted models were chosen for refinement and validation. The stereochemical quality of protein structures were analyzed utilizing several web tools to enhance the accuracy of evaluation. MolProbity, PROCHECK, VADAR, VERIFY3D, SAVES, and PROSESS web tools were used for structure analysis (33-37). The structural similarity between the model and template was calculated using TM-align web server (38). Finally, the best model was selected and considered for the structure refinement using Galaxy Refine web server (39).

Molecular dynamics simulation

Protein conformational changes and stability under physiological conditions of the models were evaluated by molecular dynamics (MD) simulation using GROMACS 4.6.5 package with Amber99SB-ILDN force field (40). The system was generated by solving protein in a cubic box with 1nm distance from the edges and TIP3P model as the water model during all simulations (41). The net charge of the system was neutralized by replacing water molecules with proper number of Cl^- and Na^+ ions. The system energy minimization was conducted by taking advantage of steep- descent with a tolerance of 10 kJ/mol/nm in 500,000 steps, and the periodic boundary condition in x, y, and z directions. It was equilibrated in the canonical (NVT) and isothermal –isobaric (NPT) ensembles using the verlet algorithm with an integration time step of 0.01 ps. A 1.2 nm cut off was set for Coulomb interactions,

[Downloaded from ijmcmed.org on 2026-11-12]

[DOI: 10.22088/IJMCM.BUMS.9.1.90]

and particle mesh ewald (PME) was applied for long-range electrostatic calculations (42). Final equilibrated systems were subjected to MD simulations for 30 ns at 300 K with 2fs time step.

Analysis of the structure and stability during simulations

Comparative analysis of time-dependent properties was performed for the trajectories according to root mean square deviation (RMSD), root mean square fluctuation (RMSF), solvent accessible surface areas (SASA), and radius of gyration. The electrostatic energy was calculated for the structures to confirm the stability of protein–PSA during simulations.

Molecular docking and protein–ligand interact-tions

Docking a ligand into the binding site of a receptor and estimating the binding affinity of the complex is an important part of the computational drug design (43). Three dimensional structure of uric acid as ligand was extracted from crystal structure of *Aspergillus flavus* with PDB ID: 4D12 (44). To predict the binding affinity of various uricase-PAS fusions, docking into uric acid was conducted with AutoDock 4.2 (Scripps Research Institute). First, the receptor and ligand file preparations were carried out by the plugin using scripts from the Autodock Tools package. Lamarckian genetic algorithm was employed for docking simulations (45). A grid box of 60, 40, and 60 points in x, y, and z directions was defined with a grid spacing of 0.375 Å. Then, the default settings were used for all other parameters. Finally, the output file was analyzed for free energy of ligand binding (ΔGbinding, kcal/mol) and the best poses were mapped using Ligplot^{+} to find H- and non-H bonds of receptor-ligand (46). The macromolecular structures were visualized by Py-MOL (the PyMOL Molecular Graphics System) program (47).

Results

Uricase showed a highly conserved sequence

The multiple sequence alignment indicated that uricase possesses a highly conserved sequence among different species of *Aspergillus*. The result revealed that the level of residue conservation for both C- and N- terminal region of protein was higher than internal regions (Fig1.C). Analysis of the phylogenetic tree exhibited a rather close relation among *Aspergillus* species (Fig1.B). The multiple sequence alignment of the PAS sequences determined seven repetitive blocks of PAS, which are listed in Table 1.

Designed PAS sequences indicated distinct physiochemical properties

The calculated pI of various PAS sequences revealed their acidic character (5.57). However, the designed PAS sequences had no charge at neutral pH. The instability index presents an estimate of the stability of protein in which a value above 40 predicts that the protein may be unstable (48). The instability index values of sequences referred to their instability. The maximum instability was related to sequences of PAS#4 (247.73), while, the minimum was for PAS#5 sequences (142.50). It can be seen that sequence composition has affected the stability; whereas lower percentage of Pro and Ser resulted in lower instability index values, the ratio1:2 Seri:Prol has led to the most sequence stability. The GRAVY value was calculated as the sum of hydropathy values of all the amino acids, divided by the number of residues in the sequence (49). The lower value reflected the characteristics of a soluble sequence whereas the more positive value was related to hydrophobic sequence. Indeed, PAS#3N and PAS#4 had more hydrophilic properties compared to other sequences. More details about physicochemical properties such as molecular weight and residue composition of designed PAS sequences are provided in Table 2.

The three-dimensional structural model of uricase-PAS fusions were validated for further analysis

[Downloaded from ijmcmed.org on 2026-11-12]

[DOI: 10.22088/IJMCM.BUMS.9.1.90]

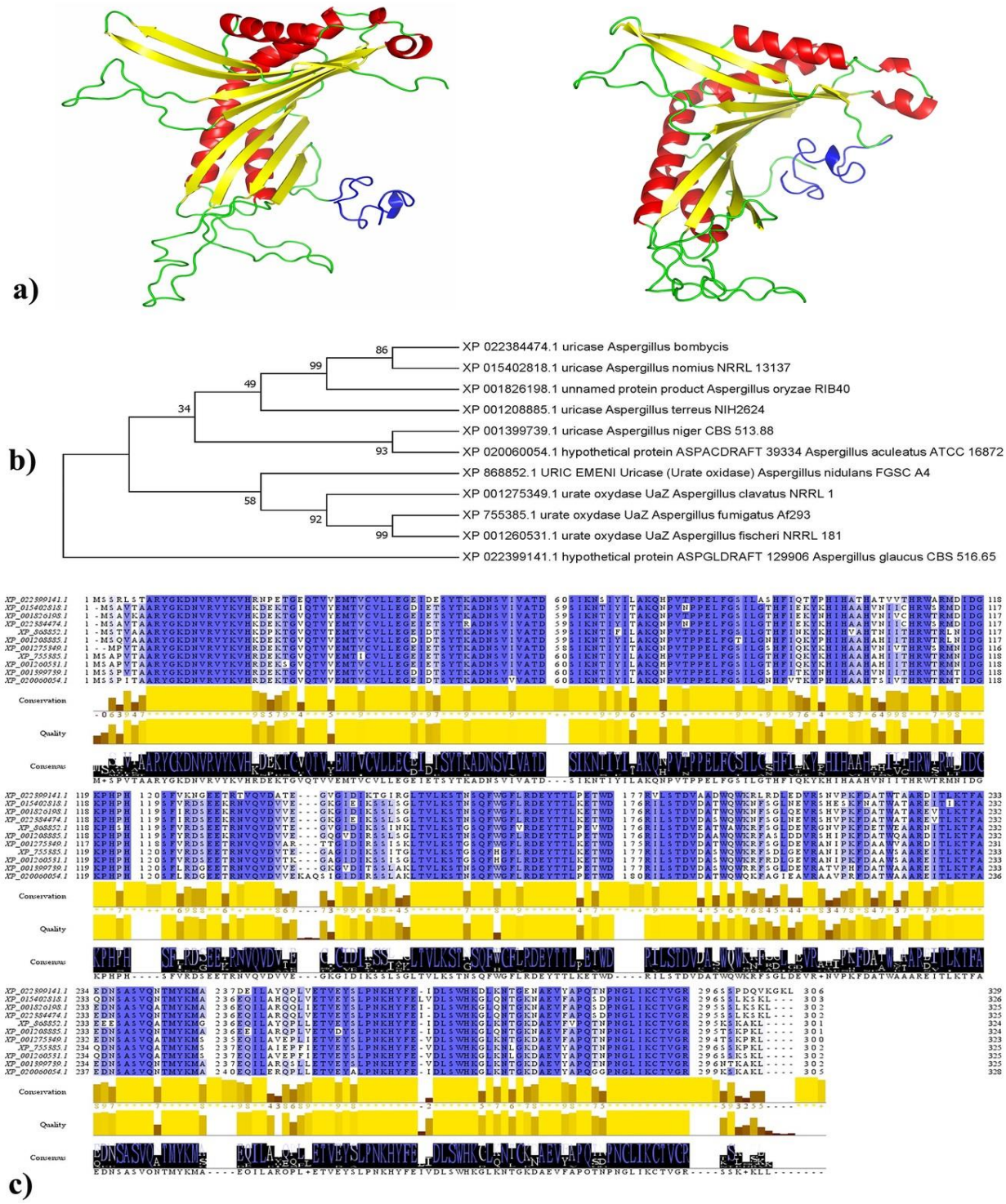


Fig. 1. **Characteristics of uricase-PAS fusions.** a: 3D structures of final refined uricase-PAS5; residues are colored based on their structure along the chain, alpha-helix (red), beta-sheets (yellow), loops (green), and PAS5 at the C-terminal end (blue); b: phylogenetic tree of uricasesequences. The sequences were aligned and compared based on neighbor joining method with bootstrapping to provide confidence for tree topology. The percentage of replicate trees in which the associated taxa clustered together in the bootstrap values (1,000 replicates) has been depicted next to the branches; c: multiple sequence alignment; the representation style of coloring was by percentage identity scheme, which used conservation and consensus analysis for multiple sequence alignment in the Jalview.

[Downloaded from ijmcmed.org on 2026-11-12]

[DOI: 10.22088/IJMCM.BUMS.9.1.90]

Table 2. Physiochemical properties of designed PAS sequences.

Sequence ID	Length	MW	Total charge	Pi	P%	S%	A%	GRAVY	Instability Index
PAS#1	20	1669.85	0	5.57	35	15	50	0.22	169.00
PAS#1-40	40	3321.69	0	5.57	35	15	50	0.22	169.25
PAS#1-75	75	6201.9	0	5.57	14.7	34.7	50.7	0.24	169.73
PAS#1-100	100	8277.21	0	5.57	35	15	50	0.22	169.4
PAS#1-300	300	24795.61	0	5.57	35	15	50	0.22	169.47
PAS#1-500	500	41314	0	5.57	35	15	50	0.22	169.48
PAS#2	20	1669.85	0	5.57	35	15	50	0.22	156.66
PAS#3N	20	1781.85	0	5.57	35	50	15	-0.69	234.91
PAS#4	20	1781.85	0	5.57	35	50	15	-0.69	247.25
PAS#5	24	1996.21	0	5.57	33.3	16.7	50	0.23	142.50

MW: molecular weight; P: proline; S: serine; A: alanine; GRAVY: grand average of hydropathicity.

Table 3. First part of validation results of predicted 3D models for uricase-PAS fusions.

Uricase-PAS fusions	Verify 3D (%) [1]	Procheck Gfactor (all)[2]	Ramachandran plot quality (%)				Overall quality[3]
			Most favored	Additionally allowed	Generously allowed	Disallowed	
PAS1-40-uricase	79.18	-0.3	93.40	5.60	0.70	0.30	4.5
PAS1-75-uricase	81.65	-0.53	92.00	6.20	0.60	1.20	4.5
PAS1-100-uricase	92.77	-1.24	88.80	10.30	0.60	0.30	3.5
PAS1-300-uricase	93.01	-2.01	85.70	11.50	0.90	1.90	3.5
PAS1-500-uricase	91.64	-3.13	87.00	9.80	1.80	1.30	3.5
PAS2-uricase	85.67	0.18	95.50	4.20	0.30	**0.00**	**6.5**
PAS4-uricase	88.79	0.59	95.50	3.50	0.70	0.30	**6.5**
PAS5-uricase	88.31	0.59	94.50	4.80	0.30	0.30	4.5
Uricase-PAS1	86.60	0.3	**96.20**	2.80	0.70	0.30	**6.5**
Uricase-PAS1-40	84.75	0	95.00	4.30	0.70	**0.00**	4.5
Uricase-PAS1-75	85.64	-0.24	91.70	7.10	0.60	0.60	4.5
Uricase-PAS1-100	87.78	-1.42	88.20	10.60	0.60	0.60	4.5
Uricase-PAS1-300	**94.34**	-1.83	86.40	11.10	1.30	1.30	3.5
Uricase-PAS1-500	91.51	-2.72	87.00	9.80	1.70	1.50	3.5
Uricase-PAS2	73.52	0.35	95.80	3.80	0.30	**0.00**	**6.5**
Uricase-PAS3N	85.67	**0.65**	94.80	4.90	0.30	**0.00**	**6.5**
Uricase-PAS4	80.69	0.59	95.10	4.90	0.00	**0.00**	**6.5**
Uricase-PAS5	83.08	0.47	95.90	4.10	0.00	**0.00**	**6.5**

1-100 is the best, 0 is the worst 2- Score higher than −0.5 is in general an indication of a good quality model 3-10 is the best, 0 is the worst

There was no experimentally solved 3D structure for repetitive motifs of designed PAS sequences. Therefore, *ab initio* modeling approach was employed to generate 10000 models for each unique PAS sequence using Rosetta3.4 package. After refinement of models, Modeller predicted the full-length structure of different combinations of uricase-PAS sequence fusions. The stereochemical quality of top predicted structure of fusions is reported in Table 3. First, compatibility of the 3D model was analyzed based on the amino acid sequence using Verify3D. A well compatible 3D structure is defined when more than 80% of the amino acids are scored ≥ 0.2. Furthermore, results from PROCHECK Ramachandran plots showed the divergent values of most favored and disallowed

[Downloaded from ijmcmed.org on 2026-11-12]

[DOI: 10.22088/IJMCM.BUMS.9.1.90]

regions from 85.70%-96.20%, and from 0% to 1.90%, respectively. It revealed that the stereochemical quality of some fusion models was satisfactory, and an acceptable percentage of residues was located in the most favored region. A model with an overall scores of PROCHECK G-factor higher than −0.5 is accepted in general as an indication of a good quality model (36). Besides, the overall quality of final models was measured using PROSESS web servers. The higher score in the range of zero to 10 admitted the overall quality of final model (Table 3). In terms of considering the major geometrical aspects of protein, QMEAN estimates the quality of predicted models compared to the experimental structures. It stands for qualitative model energy analysis, and the more positive values indicate the higher quality of model (50). Negative values signify that the models have scored lower than experimental structures on average (Table 4). Next, the non-bonded atomic interactions of models were assessed based on the ERRAT value as an overall quality factor with a score above 50 representingthe reliability and quality of models (Table 4).

Concerning the topological similarity of two proteins, TM-score is a metric of the global fold similarity. It is measured as a value in range of 0, 1, where one denotes a perfect match between two structures. The TM-values of predicted models compared to the template 3D structure (4D12) revealed the folding similarity of models with the template with the score of 0.81453. A score higher than 0.5 is generally assumed as similar structures' folding (Table 4).

Then, the number of steric clashes that arises due to the unfavorable overlap of any two-nonbonding atoms in a protein structure, were reported as Molprobity score (34). Better models possess a lower number of clash scores. The clash score of uricase–PAS sequence fusions were in

Table 4. Second part of validation results of predicted 3D models for uricase-PAS fusions.

Uricase-PAS fusions	QMEAN[1]	ERRAT (%) [2]	TM-score[3] to 4D12	MolProbity score^[4]	VADAR Free energy of folding	ProSA[5] Z-score
PAS1-40-uricase	-2.15	74.7748	0.81453	2.67	-277.20	-5.37
PAS1-75-uricase	-1.24	65.6676	0.81453	2.46	-288.91	-5.4
PAS1-100-uricase	-1.10	64.433	0.81453	2.62	-316.60	-5.86
PAS1-300-uricase	-1.19	48.5618	0.81453	2.58	-403.02	-7.21
PAS1-500-uricase	-2.06	36.8421	0.81453	2.97	**-626.51**	-5.37
PAS2-uricase	-1.19	75.6494	0.81453	2.21	-255.44	-6.5
PAS4-uricase	-1.06	82.0847	0.81453	**1.98**	-238.65	-6.14
PAS5-uricase	-1.50	79.1798	0.81453	2.07	-257.25	-6.16
Uricase-PAS1	-1.71	80.7947	0.81453	2.28	-241.37	-5.94
Uricase-PAS1-40	-1.24	78.012	0.81453	2.25	-271.12	-5.85
Uricase-PAS1-75	**-0.88**	73.4247	0.81453	2.31	-286.14	-5.99
Uricase-PAS1-100	-1.08	64.0306	0.81453	2.9	-313.66	-5.94
Uricase-PAS1-300	-1.11	46.9492	0.81453	2.5	-398.78	**-7.71**
Uricase-PAS1-500	-1.76	43.9532	0.81453	2.67	-591.77	-6.14
Uricase-PAS2	-1.60	82.0513	0.81453	2.19	-251.34	-6.19
Uricase-PAS3N	-1.03	84.0391	0.81453	2.3	-256.35	-6.22
Uricase-PAS4	-1.01	80.7692	0.81453	2.25	-236.89	-5.94
Uricase-PAS5	-0.90	**85.7605**	0.81453	2.31	-254.53	-6.78

QMEAN: qualitative model energy analysis; VADAR: volume area dihedral angle reporter; 1- The higher QMEAN score, the more similarity to the experimental structures of similar size. 2- 100 is the best, 0 is the worst. 3- TM-score has the value in (0, 1]. The higher score assumes generally the same folding. 4- MolProbity score^ combines the clashscore, rotamer and Ramachandran evaluations into a single score. 5- ProSA Z-score determines the overall model quality.

[Downloaded from ijmcmed.org on 2026-11-12]

[DOI: 10.22088/IJMCM.BUMS.9.1.90]

Table 5. Physiochemical properties of uricase-PAS fusions.

Sequence ID	Length	MW	pI	-R	+R	Half-life (hours)	GRAVY	Instability Index
Uricase	301	34109.57	7.16	37	37	1.9	-0.465	37.34
PAS1-40-uricase	341	37413.2	7.34	37	37	**4.4**	-0.385	52.84
PAS1-75-uricase	376	40293.46	7.34	37	37	**4.4**	-0.324	63.77
PAS1-100-uricase	401	42368.77	7.34	37	37	**4.4**	-0.294	70.30
PAS1-300-uricase	601	58887.17	7.34	37	37	**4.4**	-0.123	103.31
PAS1-500-uricase	801	75405.56	7.34	37	37	**4.4**	-0.037	119.84
PAS2-uricase	321	35761.41	7.34	37	37	**4.4**	-0.422	45.41
PAS4-uricase	321	35873.41	7.16	37	37	1.9	-0.479	50.45
PAS5-uricase	325	36087.77	7.34	37	37	**4.4**	-0.414	45.14
Uricase-PAS1	321	35761.41	7.16	37	37	1.9	-0.422	45.41
Uricase-PAS1-40	341	37413.25	7.16	37	37	1.9	-0.385	52.84
Uricase-PAS1-75	376	40293.46	7.16	37	37	1.9	-0.324	63.77
Uricase-PAS1-100	401	42368.77	7.16	37	37	1.9	-0.294	70.30
Uricase-PAS1-300	601	58887.17	7.16	37	37	1.9	-0.123	103.31
Uricase-PAS1-500	801	75405.56	7.16	37	37	1.9	-0.037	119.84
Uricase-PAS2	321	35761.41	7.16	37	37	1.9	-0.422	44.81
Uricase-PAS3N	321	35873.41	7.16	37	37	1.9	-0.479	49.68
Uricase-PAS4	321	35873.41	7.16	37	37	1.9	-0.479	50.45
Uricase-PAS5	325	36087.77	7.16	37	37	1.9	-0.414	45.14

MW: molecular weight; GRAVY: grand average of hydropathicity; -R: total number of negatively charged residues (Asp+Glu); +R: total number of positively charged residues (Arg+Lys).

ranges from 1.98 to 2.97 that was acceptable (Table 4). Together with this, volume area dihedral angle reporter (VADAR) evaluates key structural parameters of proteins. It calculates free energy of overall fold quality. The lower free energy indicated higher quality of protein folding.The amounts of energies admitted the quality of the structures consistent with other programs (Table 4).

Finally, the Z-score values for predicted structures were in ranges of -7.71 to -5.37, which were within the range observed for native set of proteins of the same sizes. The Z-score outside the range of native proteins found by X-ray and NMR, indicates an erroneous structure (Table 4). Overall, the 3D structure of uricase-PAS5 was depicted in Fig 1. A as an example of validated models.

Fusions with PAS sequences at N-terminal indicated extended half-life

The calculated pI of fusions showed a natural physiological character (7.16-7.34). However, the total number of negatively and positively charged residues of all structures was equal at neutral pH. As previously mentioned, the instability index values of proteins referred to their instability. The maximum instability was related to PAS1-500-uricase and uricase-PAS1-500 (119.84) and the minimum was for PAS5-uricase and uricase-PAS5 (45.14). It can be seen that longer PAS sequence has affected the stability; whereas smaller sequences resulted in lower instability index values. The negative GRAVY value of proteins reflected their hydrophilic characteristics.Nevertheless, fusions with smaller PAS sequences showed more hydrophilic properties in comparison with longer ones. In terms of half-life, N-terminally PASylated uricase displayed prolonged duration period (4.4 h). More details about physicochemical properties such as molecular weight and length of uricase-PAS structures are provided in Table 5.

RMSD evaluations showed that the least deviation belonged to PAS1-40-uricaseand PAS 2-uricase fusions

The root mean square deviations of the backbone of fusions compared to their initial

[Downloaded from ijmcmed.org on 2026-11-12]

[DOI: 10.22088/IJMCM.BUMS.9.1.90]

conformation were calculated to estimate the structure stability. The RMSD value against the simulation period (30 ns) is depicted in Fig 2. The plot showed fluctuations and plateau states (15 ns) of all models except for uricase-PAS1-300 which displayed the minimum changes. As can be seen the least deviations belong to PAS1-40-uricase and PAS2-uricase with the most structure stability whereas the uricase-PAS1-300 having the most fluctuations and deviation showed the least constancy. Furthermore, analysis of backbone deviation of models whether PAS sequences were added to the N- or C- terminal of uricase showed that the structure of predicted models with PAS1-40, PAS1-75 and PAS5 has converged towards an equilibrium state in the same pattern for both PAS positions (Fig 2. B-C-F). Besides, the structure of predicted models with PAS1-500 and PAS2 at N-terminal position of uricase has achieved fewer deviation compared to models with PAS at C-terminal (Fig 2. D-E). However, the other models displayed higher fluctuation of RMSD values during MD simulation without noticeable convergence (Fig 2. A).

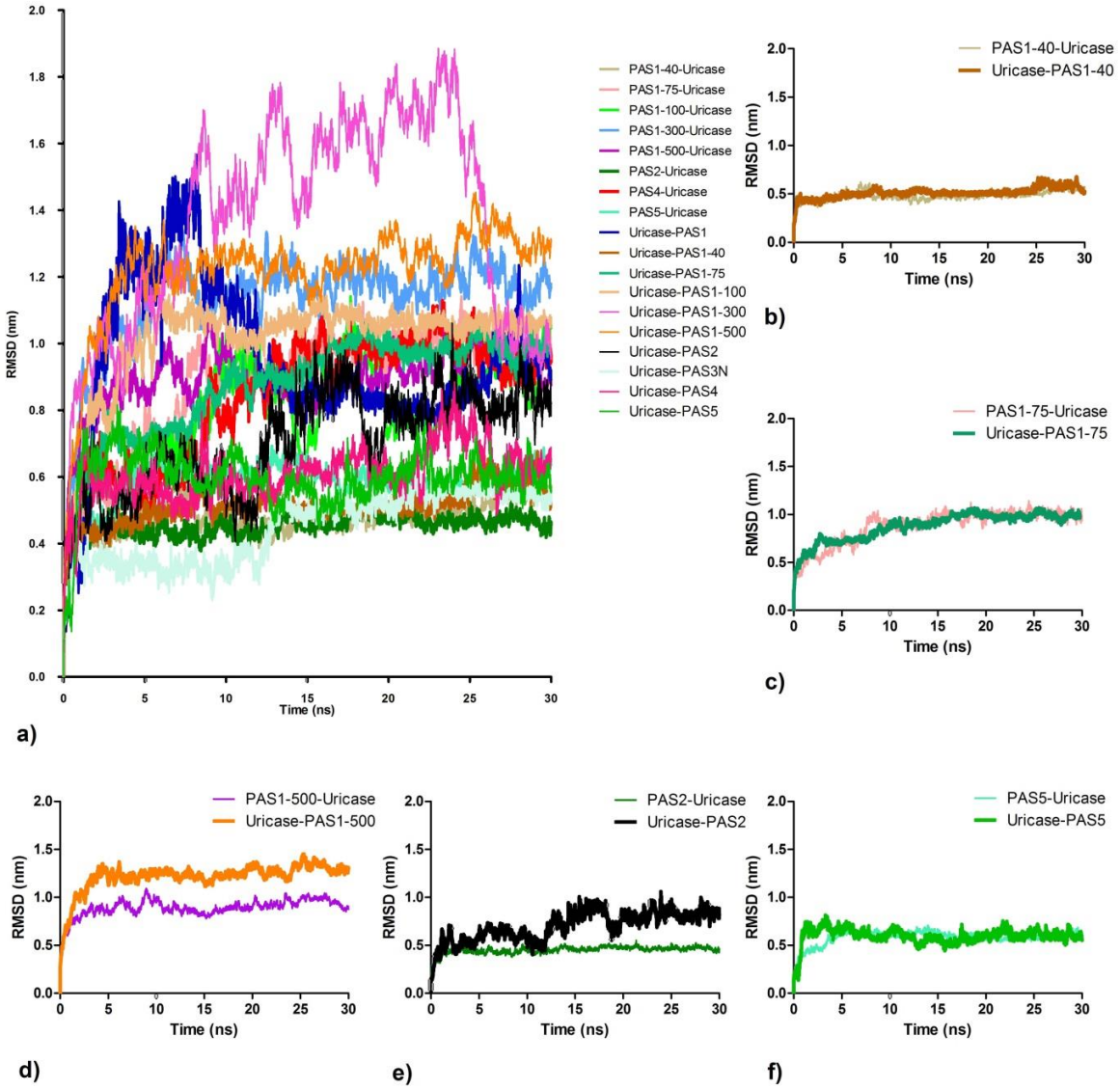


Fig. 2. Analysis of molecular dynamics (MD) simulations for fusions. a: the root mean square deviation (RMSD) plots of PASylated uricase; b: the RMSD plots of PAS1-40-Uri, Uri-PAS1-40 (c): PAS1-75-Uri, Uri-PAS1-75; d: PAS1-500-Uri, Uri-PAS1-500; e: PAS2-Uri, Uri-PAS2; f: PAS5-Uri, Uri-PAS5 that show their convergence after MD simulation (Using prism software).

[Downloaded from ijmcmed.org on 2026-11-12]

[DOI: 10.22088/IJMCM.BUMS.9.1.90]

Fusion residues in models with N-terminallyPAS sequences possess less fluctuation

The average fluctuation of each residue during simulation was calculated as the RMSF of the Cá atoms. The results were plotted for each model to display residue fluctuations of fusions and the PAS sequences distinctively (Fig 3 and 4). The RMSF values indicate the flexibility of each residue, which are comparable to X-ray B-factors (51). Analysis of RMSFs pattern revealed that fusion residues in models with PAS sequences located at N-terminal region had less flexibility in comparison with the other models. However, it seems that the length of PAS sequences at C-terminal region has affected the amount of residue fluctuations. While the predicted models with PAS1-40, PAS1-75, PAS2, PAS3N, PAS4, and PAS5 sequences at both C- and N-terminal regions have shown the minimum residue fluctuation (0.5 nm), the presence of PAS1-100, PAS1-300 and PAS1-500 at C-terminal region

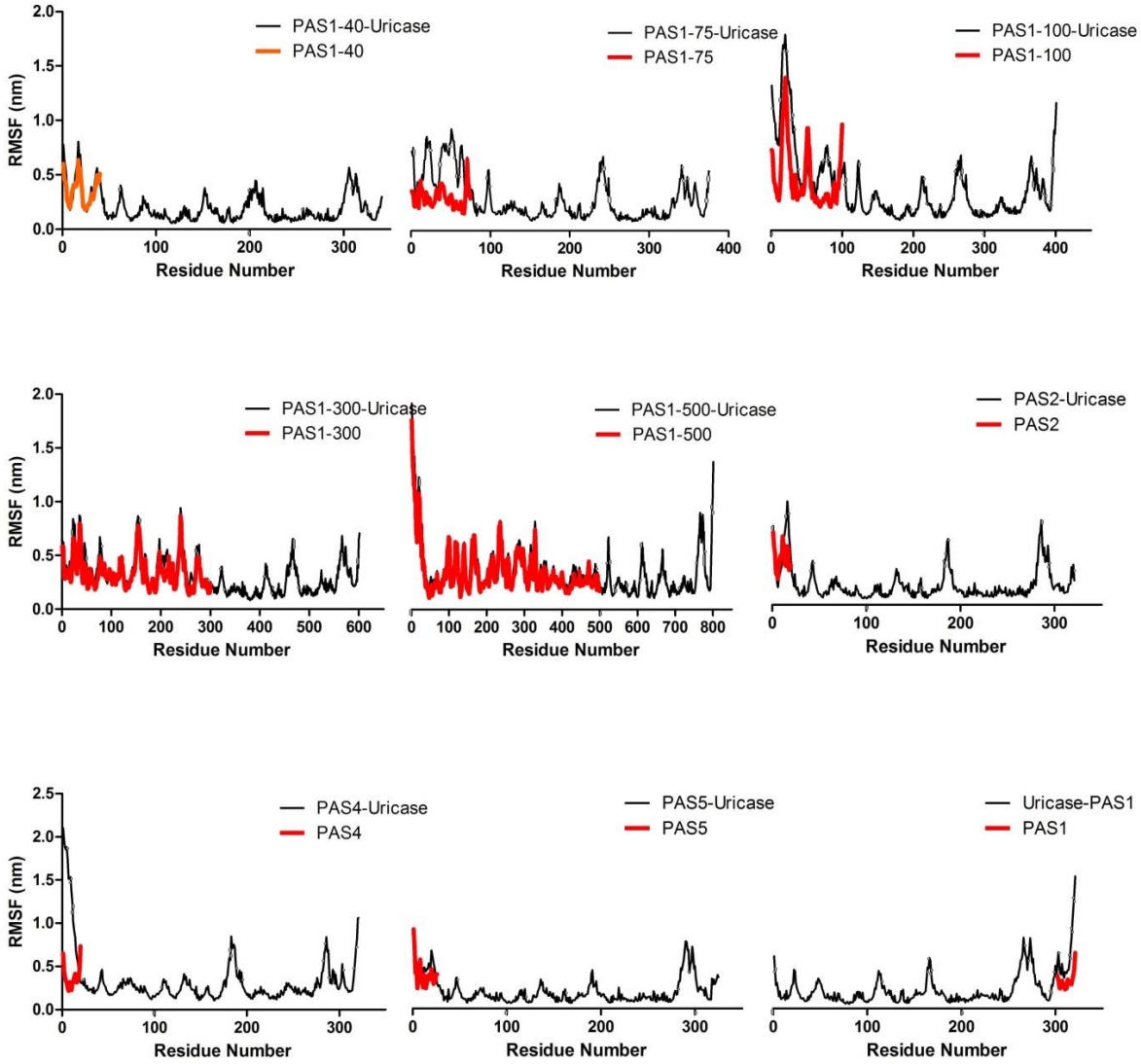


Fig. 3. The root mean square fluctuation (RMSF) plots of N-terminally PASylated uricase fusions and their PAS amino acids. The last plot related to uricase PASylated at C-terminal end. Red lines are indicative of PAS sequences (Using prism software).

[Downloaded from ijmcmed.org on 2026-11-12]

[DOI: 10.22088/IJMCM.BUMS.9.1.90]

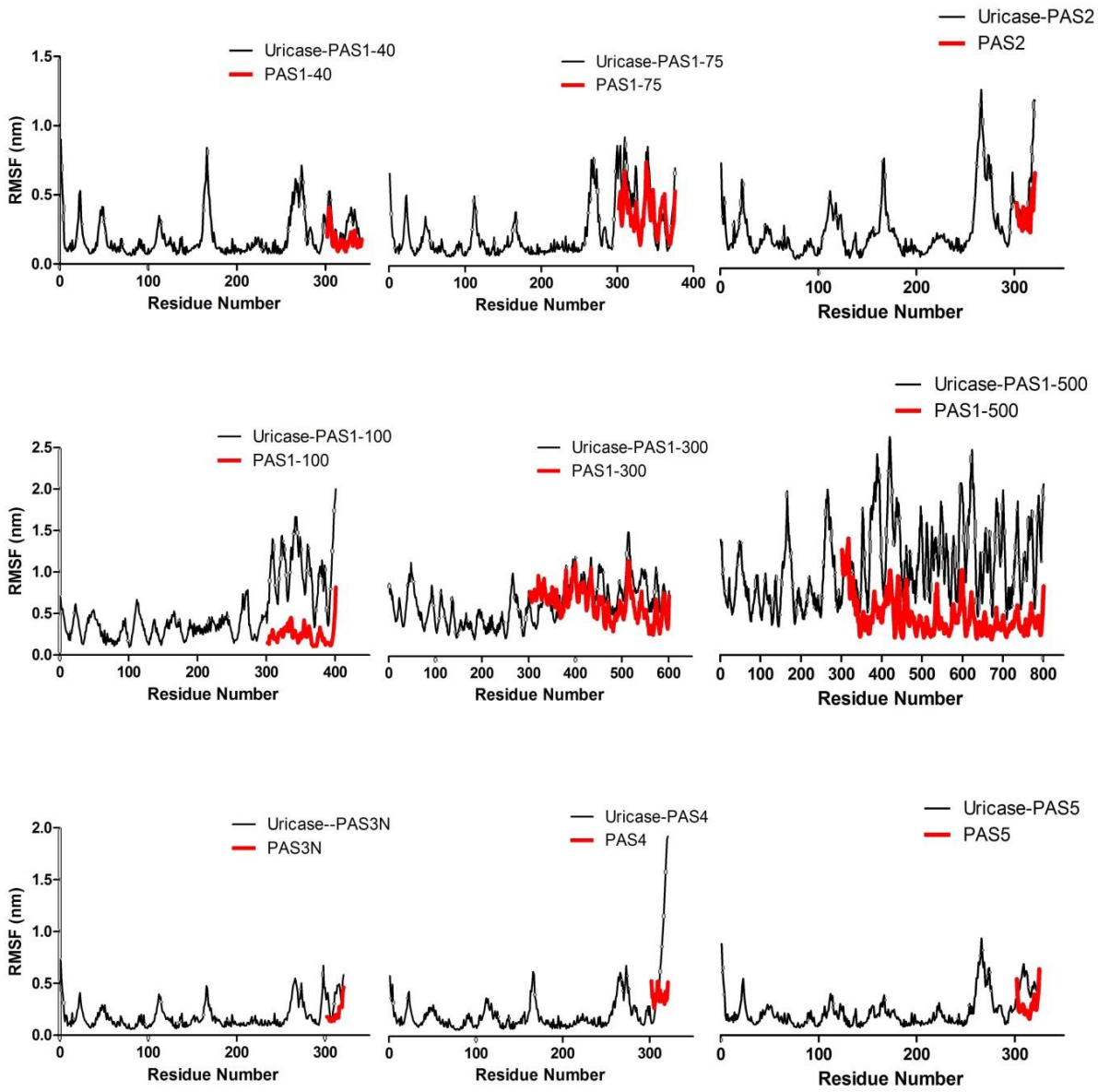


Fig. 4. The root mean square fluctuation (RMSF) plots of C-terminally PASylated uricase fusions and the PAS sequences. Red lines are indicative of PAS sequences (Using prism software)..

has increased RMSF scores.

The radius of gyration (RoG) evaluations showed that the length of PAS sequences has influenced the fusion compactness

RoG is a sign of protein structure compactness and constancy. Analysis of the results revealed that fusion structures with PAS sequences from 20 to 100 residues were more compacted in comparison with longer sequences (300 and 500 residues). While, the RoG value of the former was around 2.5 nm, the latter showed RoG to be above 4 nm. Calculation of PAS sequences individually as index of fusion structure indicated that the PAS2 had the lowest RoG value (on average 0.5 nm) in comparison with other PAS sequences in the same size. Interestingly, the compactness of short PAS sequences (PAS1, 2, 3N, 4, and 5) was higher when they were located at C-terminal region of fusions (average RoG values of 1.2, 0.5, 0.7, 1.0, and 0.8 nm, respectively).

[Downloaded from ijmcmed.org on 2026-11-12]

[DOI: 10.22088/IJMCM.BUMS.9.1.90]

The accessibility of surface into solvent has increased by longer PASsequences

The solvent-accessible surface area (SASA) is the surface area of a biomolecule that is attainable to a solvent.Higher scores predict that molecules are more sticking out into solvent, whereas, lower scores mean that the molecule is more buried in the protein. Analysis of fusions demonstrated that SASA values were increasing when the structures possessed longer PAS sequences. The maximum score was related to uricase-PAS1-500 with 426.27 (nm\S2\N) (Table 6). Furthermore, the similar values of area per atom and residue for all fusions could be interpreted as no significant effect of different length and position of PAS sequences on average area per atom and residue (Table 6).

The length of PAS sequences has affected the fusion energies and volume

The potential energy value gives the energy of the system as a function of the positions of the atoms referring to the consistency of a macromolecule in solution. Analysis of the simulation systems of all fusions revealed that the structures have reached to the constant values of energy after 5ns of simulations. The fusions with longer PAS sequences gained the lowest amount of energy (uricase-PAS1-500: -7.38×106 kJ/mol) (Table 6). Besides, analysis of electrostatic energy of fusions was consistent with the potential energy values. The longer length of PAS sequences has affected the fusion electrostatic energy. While the fusions with sequences of 20 to 100 residues showed the similar Coulomb energy, the lowest amount of energy belonged to uricase-PAS1-500 at -7.38×106 kJ/mol (Table 6).

In terms of free volume, the results showed that all fusions had similar value around 42%. Additionally, the hydrodynamic volume of fusions as expected was increasing by raising the PAS sequence length. Therefore, the highest volume was

Table 6. Molecular dynamic analysis of predicted 3D models for uricase-PAS fusions.

Uricase-PAS fusions	SASA (nm\S2\N)	Average area per atom (nm\S2\N)	Average area per residue (nm\S2\N)	Volume and density (nm\S3\N)	Coulomb energy (kJ/mol)	Potential energy (kJ/mol)	RMSD	RMSF	Free volume (%)
PAS1-40-uricase	198.94	0.04	0.58	70.60	-2.16×10^{6}	-1.70×10^{6}	0.62	0.81	42.18
PAS1-75-uricase	219.86	0.04	0.57	76.64	-2.14×10^{6}	-1.68×10^{6}	0.12	0.96	42.12
PAS1-100-uricase	240.84	0.04	0.58	81.50	-2.53×10^{6}	-1.98×10^{6}	0.12	1.75	42.21
PAS1-300-uricase	327.73	0.04	0.53	113.91	-4.77×10^{6}	-3.76×10^{6}	0.13	0.93	42.41
PAS1-500-uricase	414.36	0.04	0.51	145.37	-7.98×10^{6}	-6.31×10^{6}	**0.11**	0.8	42.53
PAS2-uricase	187.65	0.04	0.57	67.11	-2.78×10^{6}	-2.21×10^{6}	0.55	0.94	42.36
PAS4-uricase	199.72	0.04	0.60	68.38	-3.41×10^{6}	-2.71×10^{6}	0.12	0.76	42.46
PAS5-uricase	188.05	0.04	0.56	67.78	-2.27×10^{6}	-1.79×10^{6}	0.7	0.78	42.23
Uricase-PAS1	194.48	0.04	0.58	67.85	-2.48×10^{6}	-1.96×10^{6}	0.66	0.79	42.29
Uricase-PAS1-40	195.59	0.04	0.58	70.23	-2.44×10^{6}	-1.92×10^{6}	0.67	0.82	42.26
Uricase-PAS1-75	220.55	0.04	0.59	76.83	-2.73×10^{6}	-2.15×10^{6}	**0.11**	0.92	42.29
Uricase-PAS1-100	231.10	0.04	0.58	80.63	-2.37×10^{6}	-1.85×10^{6}	0.12	1.7	42.15
Uricase-PAS1-300	350.30	0.04	0.59	115.31	-5.32×10^{6}	-4.20×10^{6}	0.18	1.6	42.46
Uricase-PAS1-500	**426.27**	0.04	0.53	**146.34**	$\mathbf{-9.29\times10^{6}}$	$\mathbf{-7.38\times10^{6}}$	0.14	2.3	**42.59**
Uricase-PAS2	190.47	0.04	0.58	67.47	-2.30×10^{6}	-1.82×10^{6}	1	1.2	42.25
Uricase-PAS3N	189.01	0.04	0.58	67.52	-2.23×10^{6}	-1.76×10^{6}	0.6	**0.68**	42.22
Uricase-PAS4	194.62	0.04	0.58	67.84	-2.52×10^{6}	-1.99×10^{6}	0.89	0.75	42.30
Uricase-PAS5	193.41	0.04	0.59	68.26	-2.63×10^{6}	-2.08×10^{6}	0.82	0.82	42.32

SASA: solvent accessible surface; RMSD:root mean square deviation; RMSF: root mean square fluctuation .

[Downloaded from ijmcmed.org on 2026-11-12]

[DOI: 10.22088/IJMCM.BUMS.9.1.90]

Table 7. The results of uricase-PAS fusions docking to uric acid ligand.

Uricase-PAS fusions	Binding Affinity (Kcal/mol)	Number of H-bonds	Number of Non Polar Bonds
PAS1-40-uricase	-6.7	3	3
PAS1-75-uricase	-6.9	5	4
PAS1-100-uricase	-7.5	5	3
PAS1-300-uricase	-6.9	5	2
PAS1-500-uricase	-8.3	3	8
PAS2-uricase	-6	5	4
PAS4-uricase	-8	1	4
PAS5-uricase	-8.3	5	4
Uricase-PAS1	-8.6	5	4
Uricase-PAS1-40	-7.5	3	5
Uricase-PAS1-75	-7.6	**6**	5
Uricase-PAS1-100	**-8.9**	6	4
Uricase-PAS1-300	-8.5	3	5
Uricase-PAS1-500	-7.5	3	4
Uricase-PAS2	-8.5	5	5
Uricase-PAS3N	-6.8	5	5
Uricase-PAS4	-7.3	1	5
Uricase-PAS5	-8.5	2	6

related to uricase-PAS1-500 (146.34) (Table 6).

Uricase-PAS1-100 showed the highest binding affinity to uric acid

Complexes of uricase-PAS fusions and uric acid were obtained using the Autodock Tools software allowing a set of possible conformations of uric acid bound to fusions. The complexes were grouped and classified based on the most favorable binding energy. The final conformations with the lowest docked energy were chosen to predict the binding affinity (kcal/mol) of uric acid to each fusion. A more negative score indicated which of these fusions were more strongly docked with ligand. Uricase-PAS1-100 showed the highest binding affinity to the ligand (-8.9 kcal/mol). Furthermore, the interactions of uricase-PAS fusion-uric acid conformations including hydrogen and non-hydrogen bonds were analyzed using LigPlot+. The results were reported in Table 7.

Discussion

The loss of UO function in humans has made them assailable to developing the TLS (1). Rasburicase is widely used for converting uric acid to allantoin after chemotherapy of human cancers (52). However, owing to its short half-life, significant efforts have converged toward the UO stability enhancement.

In this study, we used PASylation technology to optimize hydrodynamic volume and solubility of UO. Indeed, PASylation mimics the advantageous biophysical properties of PEG that alleviate kidney filtration (21). The multiple sequence alignment of the PAS sequences determined seven repetitive blocks of PAS used to design several PAS sequences with different length (20-500 residues). They had no charge at neutral pH and the Ser, Pro 1:2 ratioin their composition has led to the most sequence stability. This can be due to the fact that

[Downloaded from ijmcmed.org on 2026-11-12]

[DOI: 10.22088/IJMCM.BUMS.9.1.90]

an appropriate mixture of Pro, Ala, and Ser in a polypeptide sequence results overall in a random coil conformation of the polymer (20). It is noteworthy that Schlapschyet al. results' indicated a collapse of the conformationally PAS sequences due to lowering the Pro content. Consequently, they proposed the importance of the Pro proportion in favorable biophysical features.

After *ab initio* modeling for each PAS sequence, the full-length structure of fused N- or C-terminally to the uricase sequence was predicted using comparative homology modeling. To determine which fusion type will be optimal for uricase, the stereochemical quality of top predicted structure of fusions was analyzed. Assessment of their properties proved appropriate quality and the success of modeling method. Subsequently, the overall quality of the structures was evaluated to obtain more qualified fusions, and reduce the clash scores. The result was consistent with the PAS sequence length, in which the shorter showed the higher quality. Besides, the biophysical behavior of PAS-fusion proteins was further investigated with regard to isoelectric and hydrophilic properties. Apart from PAS#3N and PAS#4, the PAS sequences were relatively hydrophobic. Surprisingly, we found that fused PAS sequences allowed uricase-PAS fusions exhibiting hydrophilic and highly soluble properties.

N-terminally PASylated uricase displayed extended half-life period (4.4 h). Several successful fusing of PAS polypeptides for half-life extension have been so far reported. The *in vivo* studies of fused murine leptin with PAS polypeptide revealed an increased plasma half-life from 26 min to 19.6h (53). Falvoet al. prepared PASylated human ferritin that provided increased plasma half-life of ferritin (54). Recently, Hedayati et al. showed that PASylation of a human recombinant erythropoietin (EPO-PAS) resulted in 15-fold higher circulation duration of fusion protein (55).

Molecular dynamic simulations allowed predicted 3D structures to minimize energy and form more agreeable conformations. The RMSDs of the backbone of fusions compared to their initial conformation showed convergence of models with lower number of PAS residues towards an equilibrium state in the same pattern for both N- and C-terminally PAS sequences. However, the other structures displayed higher backbone deviation during MD simulation without noticeable convergence.This can be interpreted as the tendency of longer PAS sequences to form a random coil conformation that would be the reason for the higher fluctuation of RMSD values. Moreover, analysis of RMSF patterns revealed that the length of PAS sequences has affected the average value of residue fluctuation in PASylated models.It might be caused by the large movements of residues in random coil conformation of extended PAS sequences.

Interestingly, the compactness (RoG), SASA values, the potential and electrostatic energy of fusions were increasing while the structures possessed longer PAS sequences. Radius of gyration is defined as an indicator of protein structure folding and unfolding. Therefore, a random coil conformation of extended PAS sequences is suggesting a less tight packing compared to short ones. It was also consistent with the pattern of SASA values in which the accessibility of surface into solvent has been promoted by prolonged PAS sequences.

Analytical characterization of fusion proteins showed the similar free volume (value around 42%) of all fusions and increasing the hydrodynamic volume of fusions by raising the PAS sequence length. This was consistent with the results from analysis of PAS fusion of 4D5 Fab and IFN in which a larger hydrodynamic volume has to be expected from the longer attached random coil polypeptide (56).

[Downloaded from ijmcmed.org on 2026-11-12]

[DOI: 10.22088/IJMCM.BUMS.9.1.90]

Molecular docking results revealed that the higher binding affinity to uric acid was for uricase-PAS1-100. This fusion has generated more interactions through formation of more hydrogen and non-hydrogen bonds. However, there was no significant correlation between the binding affinity and the extension of PAS sequences.

Having all these taken together, *in silico* design and analysis of uricase-PAS fusions highlighted the role of PASylation strategy to improve physicochemical properties of therapeutic proteins fused to PAS polymer with different length.

In this study, we designed and evaluated several PASylateduricase*in silico*, in which the PAS amino acid polymers with length increasing were attached either to the C- or N-terminal end of protein. Our data demonstrated that PASylation has a positive impact on stability and solubility of uricase,and potentially might extend circulation half-life of the molecule *in vitro*.

Overall, several variants of PASylated uricase were analyzed computationally to find the appropriate fusions based on physicochemical and conformational properties. 3D structures of fusions were predicted for PAS sequences in different length fused C- or N-terminally to the uricaseof *Aspergillus flavus*. The main goal was computational assessments to improve the biostability of UO using PASylation strategy. As there were no structurally characterized features to the PAS sequences, the *Ab initio* method was performed using Rosetta software. The refinement and energy minimization steps as well as molecular docking to uric acid were applied to investigate the optimization of uricase biophysical properties. Our findings would promise new insights into the production of UO with improved solubility, stability, and biological activity. With regard to the computational attempt to predict PASylated uricase, further analysis of the stability and other physicochemical properties of uricase-PAS protein would be expected *in vitro*as well as*in vivo*.

Acknowledgements

This project was a part of a Ph.D thesis and supported by the Pasteur Institute of Iran. This study was also financially supported by the Biotechnology Development Council of the Islamic Republic of Iran (Grant No.950711).

Conflict of interest

The authors declare that they have no conflict of interest.

References

1. Mughal TI, Ejaz AA, Foringer JR, et al. An integrated clinical approach for the identification, prevention, and treatment of tumor lysis syndrome. Cancer Treat Rev 2010;36:164-76.

2. Sobota J, Püsküllüoglu M, Zygulska AL. Oncological emergencies: tumor lysis syndrome. Prz Lek 2014;71:210-4.

3. Howard SC, Jones DP, Pui CH. The tumor lysis syndrome. N Engl J Med 2011;364:1844-54.

4. Cairo MS, Coiffier B, Reiter A, et al. Recommendations for the evaluation of risk and prophylaxis of tumour lysis syndrome (TLS) in adults and children with malignant diseases: an expert TLS panel consensus. Br J Haematol 2010;149:578-86.

5. Mieczkowski M, Matuszkiewicz-Rowinska J, Koscielska M. [Tumor lysis syndrome]. Wiad Lek 2015;68:664-7.

6. Jeong JH, Bae EH. Hypercalcemia associated with acute kidney injury and metabolic alkalosis. Electrolyte Blood Press 2010;8:92-4.

7. Cairo MS. Prevention and treatment of hyperuricemia in hematological malignancies. Clin Lymphoma 2002;3 Suppl 1:S26-31.

8. Lopez-Olivo MA, Pratt G, Palla SL, et al. Rasburicase in tumor lysis syndrome of the adult: a systematic review and meta-analysis. Am J Kidney Dis 2013;62:481-92.

9. Muslimani A, Chisti MM, Nadeau L, et al. How we treat tumor lysis syndrome. Oncology 2011;25.

10. Rosenberg RN, Pascual JM. Rosenberg's molecular and genetic basis of neurological and psychiatric disease. Fifth Edition ed. Boston: Elsevier; 2014.

11. Cairo MS, Bishop M. Tumour lysis syndrome: new thera-

[Downloaded from ijmcmed.org on 2026-11-12]

[DOI: 10.22088/IJMCM.BUMS.9.1.90]

-peutic strategies and classification. Br J Haematol 2004;127:3-11.

12. Wu XW, Muzny DM, Lee CC, et al. Two independent mutational events in the loss of urate oxidase during hominoid evolution. J Mol Evol 1992;34:78-84.

13. Chang BS. Ancient insights into uric acid metabolism in primates. Proc Natl Acad Sci U S A 2014;111:3657-8.

14. Legoux R, Delpech B, Dumont X, et al. Cloning and expression in Escherichia coli of the gene encoding Aspergillus flavus urate oxidase. J Biol Chem 1992;267:8565-70.

15. Ueng S. Rasburicase (Elitek): a novel agent for tumor lysis syndrome. Proc (Bayl Univ Med Cent) 2005;18:275-9.

16. Navolanic PM, Pui CH, Larson RA, et al. Elitek™–rasburicase: an effective means to prevent and treat hyperuricemia associated with tumor lysis syndrome, a Meeting Report, Dallas, Texas, January 2002. Leukemia 2003;17: 499-514.

17. Cortes J, Moore JO, Maziarz RT, et al. Control of plasma uric acid in adults at risk for tumor Lysis syndrome: efficacy and safety of rasburicase alone and rasburicase followed by allopurinol compared with allopurinol alone--results of a multicenter phase III study. J Clin Oncol 2010;28:4207-13.

18. Aronson JK. Anti-inflammatory and antipyretic analgesics and drugs used in gout. Side Effects of Drugs Annual: Elsevier; 2009. 181-215.

19. Cammalleri L, Malaguarnera M. Rasburicase represents a new tool for hyperuricemia in tumor lysis syndrome and in gout. Int J Med Sci 2007;4:83-93.

20. Binder U, Skerra A. PASylation®: a versatile technology to extend drug delivery. Curr Opin Colloid Interface Sci 2017;31:10-7.

21. Anand R, Vallooran J. Polypeptides: PASylation and XTEN. Engineering of Biomaterials for Drug Delivery Systems: Elsevier; 2018. 299-315.

22. Gebauer M, Skerra A. Prospects of PASylation(R) for the design of protein and peptide therapeutics with extended half-life and enhanced action. Bioorg Med Chem 2018;26:2882-7.

23. Chojnacki S, Cowley A, Lee J, et al. Programmatic access to bioinformatics tools from EMBL-EBI update: 2017. Nucleic Acids Res 2017;45:W550-W3.

24. Waterhouse AM, Procter JB, Martin DM, et al. Jalview Version 2--a multiple sequence alignment editor and analysis workbench. Bioinformatics 2009;25:1189-91.

25. Kumar S, Stecher G, Tamura K. MEGA7: Molecular Evolutionary Genetics Analysis Version 7.0 for Bigger Datasets. Mol Biol Evol 2016;33:1870-4.

26. Gasteiger E, Hoogland C, Gattiker A, et al. Protein identification and analysis tools on the ExPASy server. The proteomics protocols handbook: Springer; 2005. 571-607.

27. Lear S, Cobb SL. Pep-Calc.com: a set of web utilities for the calculation of peptide and peptoid properties and automatic mass spectral peak assignment. J Comput Aided Mol Des 2016;30:271-7.

28. Raman S, Vernon R, Thompson J, et al. Structure prediction for CASP8 with all-atom refinement using Rosetta. Proteins 2009;77 Suppl 9:89-99.

29. Kim DE, Chivian D, Baker D. Protein structure prediction and analysis using the Robetta server. Nucleic Acids Res 2004;32: 526-31.

30. Drozdetskiy A, Cole C, Procter J, et al. JPred4: a protein secondary structure prediction server. Nucleic Acids Res 2015;43: 389-94.

31. Bonneau R, Tsai J, Ruczinski I, et al. Rosetta in CASP4: progress in ab initio protein structure prediction. Proteins 2001;Suppl 5:119-26.

32. Soding J, Biegert A, Lupas AN. The HHpred interactive server for protein homology detection and structure prediction. Nucleic Acids Res 2005;33: 244-8.

33. Berjanskii M, Liang Y, Zhou J, et al. PROSESS: a protein structure evaluation suite and server. Nucleic Acids Res 2010;38:W633-40.

34. Chen VB, Arendall WB, Headd JJ, et al. MolProbity: all-atom structure validation for macromolecular crystallography. Acta Crystallogr D Biol Crystallogr 2010;66:12-21.

35. Willard L, Ranjan A, Zhang H, et al. VADAR: a web server for quantitative evaluation of protein structure quality. Nucleic Acids Res 2003;31:3316-9.

36. Laskowski RA, MacArthur MW, Moss DS, et al. PROCHECK: a program to check the stereochemical quality of protein structures. J Appl Crystallogr 1993;26:283-91.

37. Colovos C, Yeates TO. Verification of protein structures: patterns of nonbonded atomic interactions. Protein Sci 1993;2:1511-9.

38. Zhang Y, Skolnick J. TM-align: a protein structure alignment

[Downloaded from ijmcmed.org on 2026-11-12]

[DOI: 10.22088/IJMCM.BUMS.9.1.90]

algorithm based on the TM-score. Nucleic Acids Res 2005;33:2302-9.

39. Heo L, Park H, Seok C. GalaxyRefine: Protein structure refinement driven by side-chain repacking. Nucleic Acids Res 2013;41:-384-8.

40. Lindorff-Larsen K, Piana S, Palmo K, et al. Improved side-chain torsion potentials for the Amber ff99SB protein force field. Proteins 2010;78:1950-8.

41. Jorgensen WL, Chandrasekhar J, Madura JD, et al. Comparison of simple potential functions for simulating liquid water. J Chem Phys 1983;79:926-35.

42. Abraham MJ, Murtola T, Schulz R, et al. GROMACS: High performance molecular simulations through multi-level parallelism from laptops to supercomputers. SoftwareX 2015;1-2:19-25.

43. Yunta MJR. Docking and ligand binding affinity: uses and pitfalls. Am J Model Optim 2016;4:74-114.

44. Bui S, von Stetten D, Jambrina PG, et al. Direct evidence for a peroxide intermediate and a reactive enzyme-substrate-dioxygen configuration in a cofactor-free oxidase. Angew Chem Int Ed Engl 2014;53:13710-4.

45. Morris GM, Goodsell DS, Halliday RS, et al. Automated docking using a Lamarckian genetic algorithm and an empirical binding free energy function. J Comput Chem 1998;19:1639-62.

46. Laskowski RA, Swindells MB. LigPlot+: multiple ligand-protein interaction diagrams for drug discovery. J Chem Inf Model 2011;51:2778-86.

47. DeLano WL. Pymol: An open-source molecular graphics tool. CCP4 Newsletter on protein crystallography 2002;40:82-92.

48. Guruprasad K, Reddy BVB, Pandit MW. Correlation between stability of a protein and its dipeptide composition: a novel approach for predicting in vivo stability of a protein from its primary sequence. Protein Eng Des Se 1990;4:155-61.

49. Kyte J, Doolittle RF. A simple method for displaying the hydropathic character of a protein. J Mol Biol 1982;157:105-32.

50. Benkert P, Tosatto SCE, Schomburg D. QMEAN: A comprehensive scoring function for model quality assessment. Proteins 2008;71:261-77.

51. Fuglebakk E, Echave J, Reuter N. Measuring and comparing structural fluctuation patterns in large protein datasets. Bioinformatics 2012;28:2431-40.

52. Dinnel J, Moore BL, Skiver BM, et al. Rasburicase in the management of tumor lysis: an evidence-based review of its place in therapy. Core Evid 2015;10:23-38.

53. Bolze F, Morath V, Bast A, et al. Long-acting PASylated leptin ameliorates obesity by promoting satiety and preventing hypometabolism in leptin- deficient Lepob/ob mice. Endocrinology 2016;157:233-44.

54. Falvo E, Tremante E, Arcovito A, et al. Improved doxorubicin encapsulation and pharmacokinetics of ferritin–fusion protein nanocarriers bearing proline, serine, and alanine elements. Biomacromolecules 2016;17:514-22.

55. Hedayati MH, Norouzian D, Aminian M, et al. Molecular Design, Expression and Evaluation of PASylated Human Rec-ombinant Erythropoietin with Enhanced Functional Properties. Protein J 2017;36:36-48.

56. Schlapschy M, Binder U, Borger C, et al. PASylation: a biological alternative to PEGylation for extending the plasma half-life of pharmaceutically active proteins. Protein Eng Des Sel 2013;26:489-501.

[Downloaded from ijmcmed.org on 2026-11-12]

[DOI: 10.22088/IJMCM.BUMS.9.1.90]